Teaser:

Tributyl(methyl)phosphonium iodide is added to perovskite to form a robust grain-wrapping layer to increase solar cell stability.

Perovskite Grain Wrapping by Converting Interfaces and Grain Boundaries into Robust and Water-Insoluble Low Dimensional Perovskites

Haoyang Jiao[1], Zhenyi Ni[1], Zhifang Shi[1], Chengbin Fei[1], Ye Liu[1], Xuezeng Dai[1], and Jinsong Huang[1,2]*

[1]Department of Applied Physical Sciences, the University of North Carolina at Chapel Hill, Chapel Hill, NC, 27599, USA.

[2]Department of Chemistry, the University of North Carolina at Chapel Hill, Chapel Hill, NC, 27599, USA.

ABSTRACT

Stabilizing perovskite solar cells need to consider all defective sites in the devices. Significant efforts have been devoted to stabilizing interfaces, while stabilization of grain boundaries received less attention. Here we report a molecule tributyl(methyl)phosphonium iodide (TPI), which can convert perovskite into a wide bandgap one-dimensional (1D) perovskite that is mechanically robust, water-insoluble. Adding TPI into perovskite precursor results in a wrapping of perovskite grains with both grain surfaces and grain boundaries converted into several nanometer-thick 1D perovskites during the grain-formation process as observed by direct mapping of it. The grain wrapping passivates the grain boundaries, enhances their resistance to moisture, and reduces the iodine released during light soaking. The perovskite films with wrapped grains are more stable under heat and light. The best device with wrapped grains maintained 92.2%

of its highest efficiency after light soaking under one sun illumination for 1900 hours at 55 ℃ open circuit condition.

INTRODUCTION

With the perovskite solar cells (PSCs) at the cusp of commercialization, the instability issue of perovskite solar cells is increasingly important and urgent to be solved. Many different strategies have been applied to improve the intrinsic stability of the perovskite layers, including compositional engineering, morphology improvement, defect passivation, charge transport layer modifications, strain engineering, etc.(*1*–*6*) Incorporating metal cations such as Cs^+ was found to enhance the thermal stability and, more importantly, the light stability of methylammonium lead iodide perovskite ($MAPbI_3$).(*7*) It is also vital to stabilize the black phase of formamidinium lead iodide perovskite ($FAPbI_3$) by tuning the Goldschmidt tolerance factor toward a region in favor of a stable perovskite structure. Triple-cation (methylammonium (MA^+), formamidinium (FA^+), Cs^+) or quadruple-cation (MA^+, FA^+, Cs^+, Rb^+) and double-anion or triple anion (Br^-, I^-, Cl^-) were broadly reported to possess better thermal stability than $MAPbI_3$.(*8*, *9*) Recent studies showed that removing or dramatically reducing methylammonium cations would significantly improve perovskites thermal, chemical, and light stability.(*10*) To improve the film morphology, many solid or liquid additives such as dimethyl sulfoxide (DMSO),(*11*, *12*) carbohydrazide (CBH),(*13*) hydroxyl-substituted polyamide derivative,(*14*) n-heptylamine(*15*) in a combination of anti-solvents and annealing recipes, were used to tune the film drying and crystallization process, which effectively increased the grain sizes and improved the grain crystallinity. Surface passivation, including adding organic molecules with unique functional groups which have secondary chemical bonding with perovskites,(*16*, *17*) or converting perovskites into robust two-

dimensional perovskites,(*18–21*) oxysalts,(*22*) or sulfide,(*23*) are effective in not only passivating the surface defects but also enhancing the stability of perovskites.

Most of the strategies to improve the perovskite stability pointed out the importance of strengthening grain surfaces and grain boundaries (GBs) in polycrystalline perovskite films. The defective sites and GBs usually initialize degradation when the materials interact with moisture, oxygen, or other stressors such as high temperature, light (particularly ultraviolet light), and bias. Moisture tends to absorb protons from the ammonium cations at the GBs and then form an intermediate complex that could finally decompose.(*24*, *25*) Oxygen can attack surface iodide vacancy to form super-oxides species with the assistance of photoexcited carriers which can further damage perovskites.(*26*, *27*) Ion migration, accelerated under bias and high temperature, is generally much faster through defects such as GBs.(*28–30*) At high operational temperatures, highly-volatile species like MA^+ may depart the perovskite films from the material interfaces and GBs,(*31*) or interact with the charge transport layers, or etch electrodes. Therefore, it is essential to passivate both the interfaces and GBs and make them more robust toward all stressors, which impact not only the efficiency but also the stability of perovskite solar cells. However, most past studies only passivated the top surfaces, while the GB passivation has not been well studied. Our recent study shows that GBs have at least comparable or even more severe charge recombination rate than film surface from a direct measurement.(*32*) Compared to the material surface, the GBs are more difficult to access by passivation molecules if the surface treatment is used for passivation. Although passivation of the GBs were claimed as a result of surface treatments, it is not clear whether these surface treatment really allow the passivation molecules to penetrate the already formed grain boundaries and passivate them.(*33*, *34*) On the other hand, it is often speculated that some passivation molecules added in precursor solution would be expelled to

GBs during film formation, there was no rigorous study to determine whether these passivation molecules would really stay in GBs.(*35–38*)

In this work, we report a molecule, tributyl(methyl)phosphonium iodide (TPI), which can convert the perovskite grain boundaries to a thin and robust one-dimensional (1D) perovskite when it was added to the perovskite precursor. This one-dimensional perovskite is very stable against water/moisture, thermal, and light stressors. We directly observed the 1D perovskite could wrap the perovskite grains, resulting in improved device efficiency and much better long-term light stability for perovskite solar cells.

RESULTS

Design of grain wrapping material and its property

The protection of perovskite films by surface passivation, or even converting the perovskite surface into robust inorganic shells, might not be sufficient to protect perovskites, because degradation can precede along in-plane direction once degradation starts at some defective sites or imperfect surface protection. We propose a material structure with each perovskite grain wrapped by a thin, robust material that can be more tolerant to non-perfect passivation. It adds another barrier to lateral precession of degradation, as illustrated in **Fig.1a**. When we searched for GBs wrapping materials, we found that tributyl(methyl)phosphonium iodide (TPI) behaved very differently from many other passivation molecules. In contrast to the weak coordination bonds for many passivation molecules, TPI reacted with perovskites to partially convert it into a wider bandgap material that shows excellent water resistance.

To understand what is the reaction product, the Fourier-transform infrared spectroscopy (FTIR) and X-ray diffraction (XRD) measurements were applied to investigate the reaction

product(s) between $MAPbI_3$ and TPI, PbI_2 and TPI. We first examined the FTIR spectra of the perovskite precursor solution with TPI additive to find out whether they form complex in solution. As shown in **Fig. S1**, no peak shift or peak broadening was observed in the FTIR spectra, indicating that TPI does not strongly coordinate with $MAPbI_3$ or PbI_2 in DMF solution. This is actually important to apply TPI in device fabrication, because it would be difficult to disperse TPI to GBs if TPI reacted with perovskite precursors in solution to form insoluble substances. Then we directly mixed $MAPbI_3$ powder with TPI powder and then heated the mixture to 150 ℃. TPI melted and thoroughly mixed/reacted with the help of stirring. Then the reaction products were ground into powder for XRD measurements. We applied four different molar ratios of $MAPbI_3$:TPI from 3:1 to 1:2, considering that these ratio may be applied in perovskite solar cell fabrication. As shown in **Fig. S2**, the new diffraction peaks from the XRD patterns remained to be the same for the $MAPbI_3$:TPI mixtures with different ratios. We thus conclude that the reaction product should be the same with different perovskite:TPI ratios. When TPI was mixed with MAI or PbI_2 and heated up to 150 ℃, the same reaction product was found from the TPI : PbI_2 =1:1 mixture, while no reaction was found between TPI and MAI. To determine the product's chemical structure, we grew single crystals of the reaction product, with a photo of the crystals shown in **Fig. 1b**, light yellow strip-like crystals. A bandgap of 2.88 eV is determined from the absorption spectrum shown in **Fig. 1c**. We conducted the single crystal XRD measurement. The crystal data and structural refinement data are shown in **Table S1**(crystal data and structural refinement data for $TPPbI_3$ single crystal), which concludes that the the crystal is $TPPbI_3$. As shown by the crystal structure in **Fig. 1d**, $TPPbI_3$ is a one-dimensional perovskite which has TP^+ cations surrounding $[PbI_6]^{4-}$ one dimensional octahedral cages connected by face sharing.

We characterized the light and thermal stability of spin-coated $TPPbI_3$ films. We put the $TPPbI_3$ film and $FA_{0.91}Cs_{0.09}PbI_3$(FACs-perovskite) control film as comparison under 2.5 sun illumination in a N_2 filled box at 105 ℃ for the degradation test. Then we compared their XRD patterns before and after the heating and light soaking. As **Fig. 1e** shows, for the $TPPbI_3$ film, the intensity of the 7.49° and 10.01° peaks increased after 170 hours test, which means it had higher crystallinity, and no formation of PbI_2 was detected. It indicates the product is very stable under the light. In contrast, the whole FACs control film degrades within 6 hours as shown in **Fig. S3**. Then we annealed the bare $TPPbI_3$ films without any capping layer at 120 ℃ for 12 hours in N_2 filled glove box. As shown in **Fig. S4**, the main peak around 7.49° intensity increased significantly, indicating its crystallinity became better under 120 ℃ and other peaks almost didn't change, which means the $TPPbI_3$ has good thermal stability.

To demonstrate the protective effective of $TPPbI_3$ against water, we mixed $MAPbI_3$ and TPI powders at a molar ratio of 3:1. At this ratio, the TPI can be fully reacted and there are some $MAPbI_3$ left unreacted. The solid mixture did not show obvious change at room temperature, but the solid reaction was seen by naked eyes when they were annealed at 150 ℃ which is above the melting point of TPI (123 ℃). The white TPI power was melted and turned into a transparent liquid. After mixing with $MAPbI_3$ powder with stirring for 5 min, the liquid turned light yellow. The shell of $MAPbI_3$ particles was quickly turned into $TPPbI_3$, while some black $MAPbI_3$ at the core of these particles remained unreacted, indicating that the $MAPbI_3$ is excessive. After cooling to room temperature, the products went back to a solid state. We then soaked the powder in water. As shown in **Fig. 1f**, the powder did not show noticeable color change even after water soaking for 12 h. In striking contrast, $MAPbI_3$ powder turned yellow within 10 s when it was soaked in water. After we grounded the core/shell structured powder to expose the $MAPbI_3$ core,

it also turned yellow within 10 seconds. It shows that the formed $TPPbI_3$ shell has a strong resistance to water or moisture.

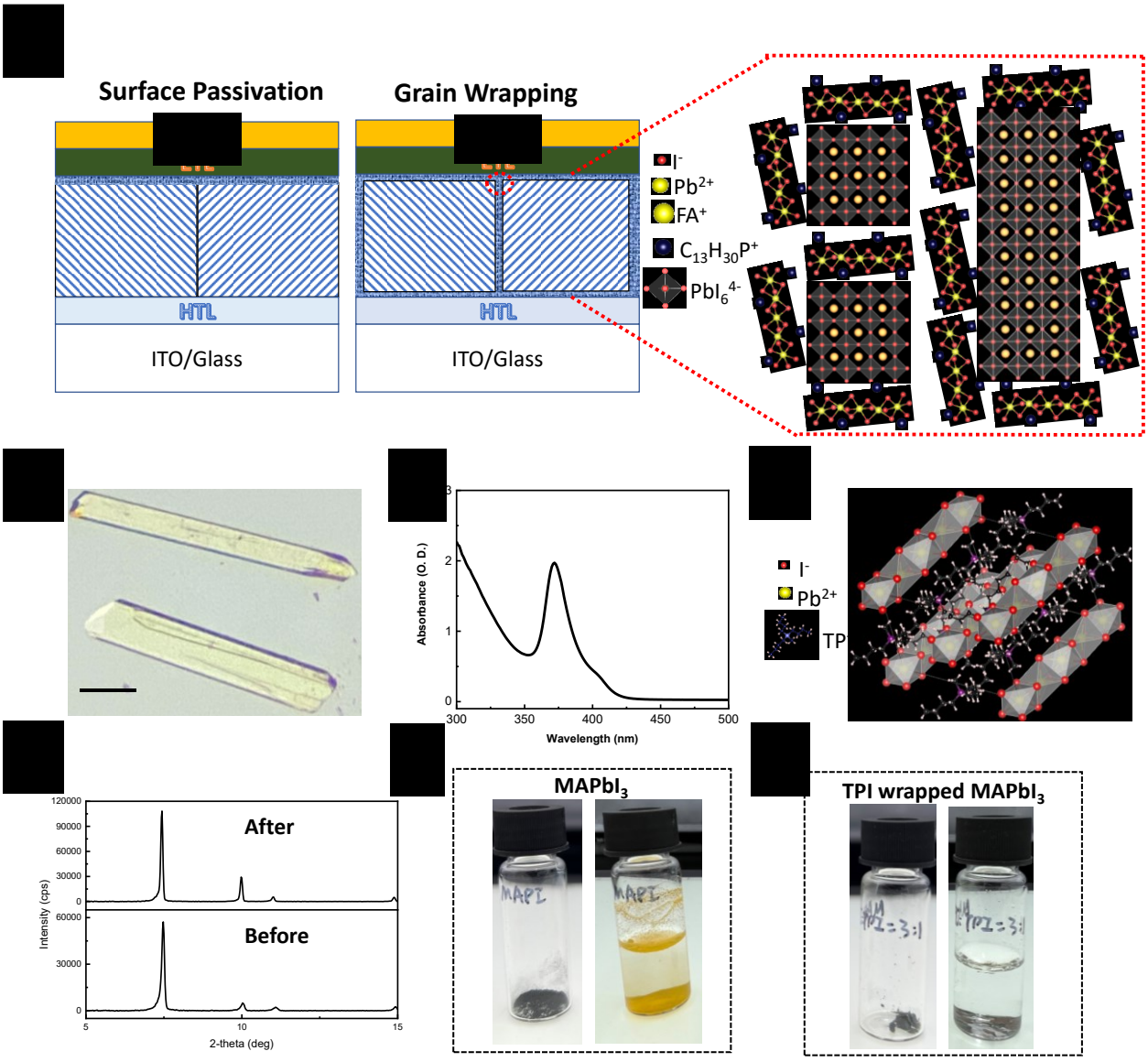

Figure 1. 1D $TPPbI_3$ for Grain Wrapping a) Schematic diagram of $TPPbI_3$ wrapped perovskite grains; b) A photograph of $TPPbI_3$ single crystals, scale bar is 0.2 mm; c) Absorption spectrum of a $TPPbI_3$ film; d) The single-crystal structure of $TPPbI_3$; e) XRD patterns of $TPPbI_3$ film before and after 2.5 sun illumination, 105 °C in N_2 degradation test for 170 hours; f) Photographs

of $MAPbI_3$ powder before and after soaking in water for 10 s; g) Photographs of $TPPbI_3$ wrapped $MAPbI_3$ before and after soaking in water for 12 hours.

We also used $MAPbI_3$ films treated by TPI for surface passivation to check whether the TPI could stabilize perovskites under illumination. We dissolved TPI into toluene (TL) and isopropyl alcohol (IPA) mixed solvent with a volume ratio of 1:4 at a concentration of 4 mM. A mixed solvent was used, because IPA dissolves TPI better, while the TL was added to reduce the damage of IPA to perovskites. After surface treatment by spin-coating TPI solution on $MAPbI_3$, both the unencapsulated control and TPI-treated $MAPbI_3$ films were illuminated by simulated sun light with an intensity of 100 mW/cm^2 in ambient air. As we can see from the XRD patterns in **Fig. S5**, the control $MAPbI_3$ film started to decompose into PbI_2 in a few minutes, and almost the whole film was converted to PbI_2 in 60 min. In contrast, PbI_2 did not show up in TPI-treated film until light soaking for 120 min. This showed that the conversation of $MAPbI_3$ surface into 1D perovskite could dramatically enhance the stability of $MAPbI_3$ against moisture under light.

Evidence of Grain Wrapping

We added TPI into precursor solation to realize grain wrapping in perovskite films. Since TP cations are too big to incorporate into the perovskite lattice, they should be expelled to the grain boundary during the perovskite crystallization process. We chose a double-cation perovskite absorber of $(FA_{0.91}Cs_{0.09})PbI_3$ (donated as FACs-perovskite), fabricated by blade coating for the device stability study because it is demonstrated much superior light and thermal stability(*39*). To find out whether TPI can really wrap the perovskite grains, we applied atomic force microscopy-based infrared spectroscopy (AFM-IR) to investigate the distribution of TP cations in the perovskite films. By measuring the thermal expansion induced by the absorption of infrared light of a chemical-bonding-specific wavelength using AFM, AFM-IR can map the

distribution of a specific moiety with the spatial resolution of regular AFM.(*40*) We first checked the FTIR signals of a control FACs-perovskite film and a pure $TPPbI_3$ film. As shown in **Fig. 2a**, we found that the strongest absorption peak of the FACs-perovskite is at 1713 $cm^{-1,}$ which can be ascribed to C=N stretching, C-H bending, or N-H bending from FA based on previous studies.(*41*) $TPPbI_3$ showed two distinguished absorption peaks at around 975 $cm^{-1,}$ and 1450 cm^{-1}, (**Fig. 2b**). The first absorption peak should be caused by $-CH_3$ rocking from TP^+, and the 1450 cm^{-1} absorption peak should come from the asymmetric $-CH_3$ stretching from TP^+.(*42*) The FTIR spectrum of TPI has both 975 cm^{-1} and 1450 cm^{-1} peaks,(*43*) confirming that they are related to TP^+ cations. To map the distribution of FACs-perovskite and TP^+ cations, we excited the samples at 1713 cm^{-1} and 975 cm^{-1}, respectively. The perovskite film in this study contains the optimal TPI amount of 0.6% molar ratio to Pb^{2+} in FACs perovskite which shows the best device performance. The topography image of the film is shown in **Fig. 2c**. As shown in **Fig. 2d**, under excitation with 975 cm^{-1} IR light, a very strong and clear response showed up at the GBs, suggesting that the grains were well wrapped by $TPPbI_3$. We estimate the thickness of the $TPPbI_3$ wrapping layer to be 1.7 nm based on a cuboid-shape grain with the size of 0.8 μm × 0.8 μm × 0.8 μm. In contrast, no clear TP^+-related signal could be observed for the control film without TPI (**Fig. 2f**). Its topography image is shown in **Fig. 2e**. When 1713 cm^{-1} IR light was used to excite the same location of the samples, a complementary distribution of perovskites could be clearly seen in **Fig. S6**. The results showed clear evidence that the $TPPbI_3$ can wrap the GBs using scalable blading fabrication.

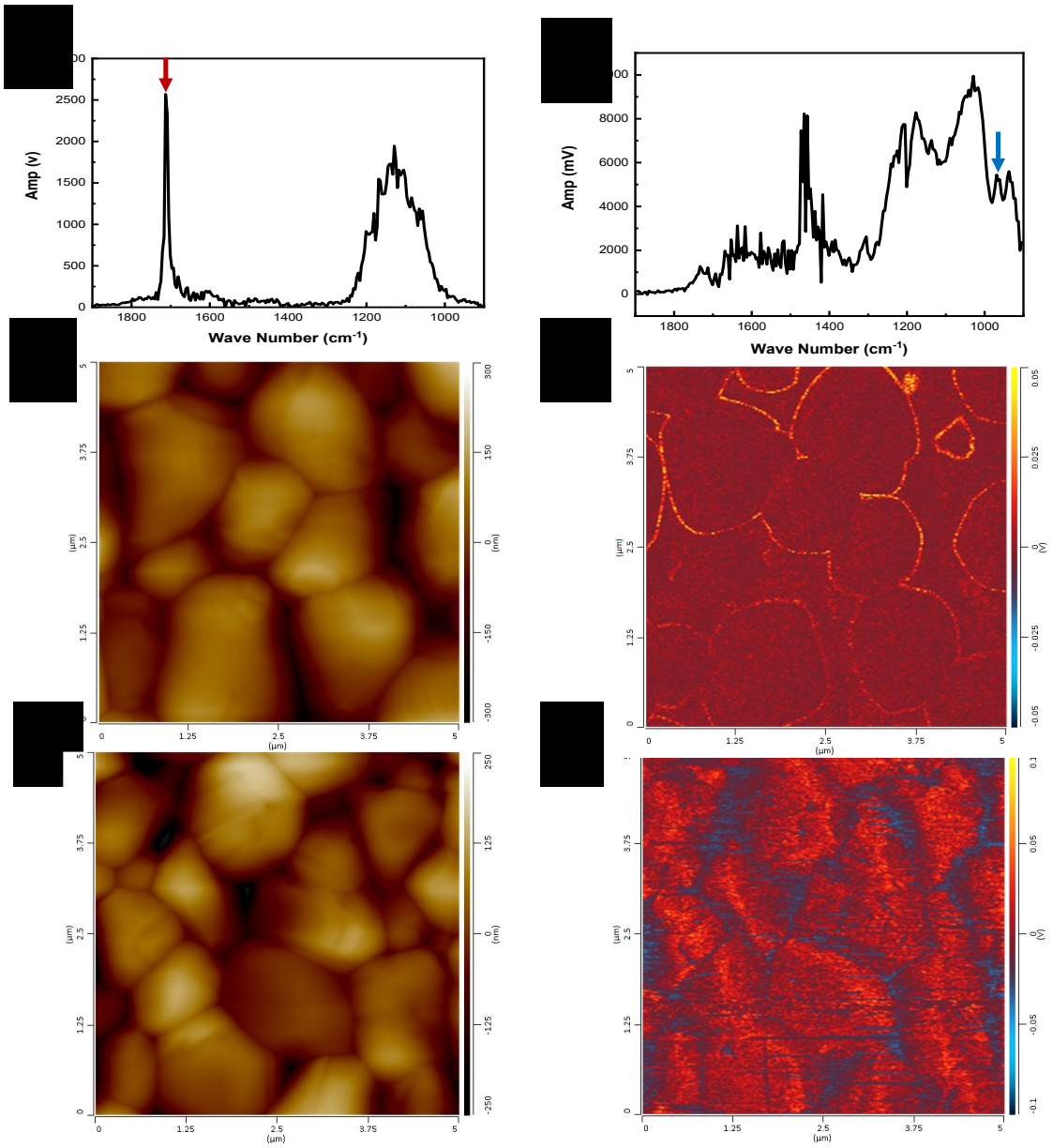

Figure 2. **AFM-IR study of perovskite films surfaces with and without TPI additive**. FTIR spectroscopy in AFM-IR equipment of a) FACs control perovskite film; b) $TPPbI_3$ film; c) Topography image of FACs perovskite film with 0.6% TPI additive; d) AFM-IR absorption of FACs perovskite film with 0.6% TPI additive at 975 cm^{-1}, corresponding to $TPPbI_3$; e) Topography image of FACs control film; f) AFM-IR absorption of FACs control at 975 cm^{-1}, corresponding to $TPPbI_3$;

We further confirm that the TPI could wrap the grains and also stay at the top and bottom surface by conducting a cross-section AFM-IR measurement. To prepare the sample, we blade-coated a layer of FACs-perovskite with 3% TPI additive on a Si substrate for a smooth cross-section, since the roughness tolerance of the AFM is less than 3 μm. The higher concentration of TPI can provide better contrast between $TPPbI_3$ and FACs-perovskite. Afterward, we blade-coated a layer of CYTOP on top of the perovskite as both perovskite encapsulant and the mechanical support for AFM tip, similar to the samples prepared for high-resolution tunneling electron microscopy (the illustration of the measurement is shown in **Fig. 3a**. The cross-sectional topography image of a sample is shown in **Fig. 3b** which shows **the** clear interface of the substrate with perovskites. **Fig. 3c** shows the phase image of the cross-section sample, where the phase contrast comes from the difference in adhesive, stiffness and frictional properties of the different materials. We determined the red region to be $TPPbI_3$, and the blue region to be FACs-perovskite. As shown in **Fig. 3d**, except for the lower phase signal area, which refers to the cleaved perovskite grain, the 975 cm^{-1} image showed the $TPPbI_3$ stayed across the whole film, while enriched at grain boundaries and interfaces of perovskites with substrate and encapsulant. The appearance of more TPI in the upper region labeled as 'A' indicates the cross-section cleaved through grain boundaries at those regions, rather than grain interior. The distribution of perovskites (**Fig. 3e**) shown by 1713 cm^{-1} excitation is almost complementary to that of $TPPbI_3$, The top surface and the bottom surface of the perovskite layer were fully covered by the $TPPbI_3$. The cross-section AFM-IR image showed complete wrapping of the grains by $TPPbI_3$. It is noted that some previous studies showed that a combination of 1D/3D heterostructure structure could improve the perovskite stability. However they were mainly limited to surface passivation.

For example, Yang, N. et al. used a cross-linking polymerizable propargylammounium (PA^+) on top of the perovskites, while no obvious evidence was shown that 1D perovskites could get into the grain boundaries.(*33*) Ge, C. et al. applied a 1D trimethyl sulfonium lead triiodide into the 3D perovskite, nevertheless still no obvious evidence showed that the 1D nanoroid could stay at the grain boundaries.(*44*) Kong, T. et. al. used 2-diethylaminoethylchloride cation to form a 1D perovskitoid as the perovskite growth templete but still no distinct evidence showed that the perovskitiod would be at grain boundaries. (*35*)Here we showed that incorporation of the 1D precursors into perovskite solution could result in the formation of a 1D wrapping layer at both grain boundaries and interfaces.

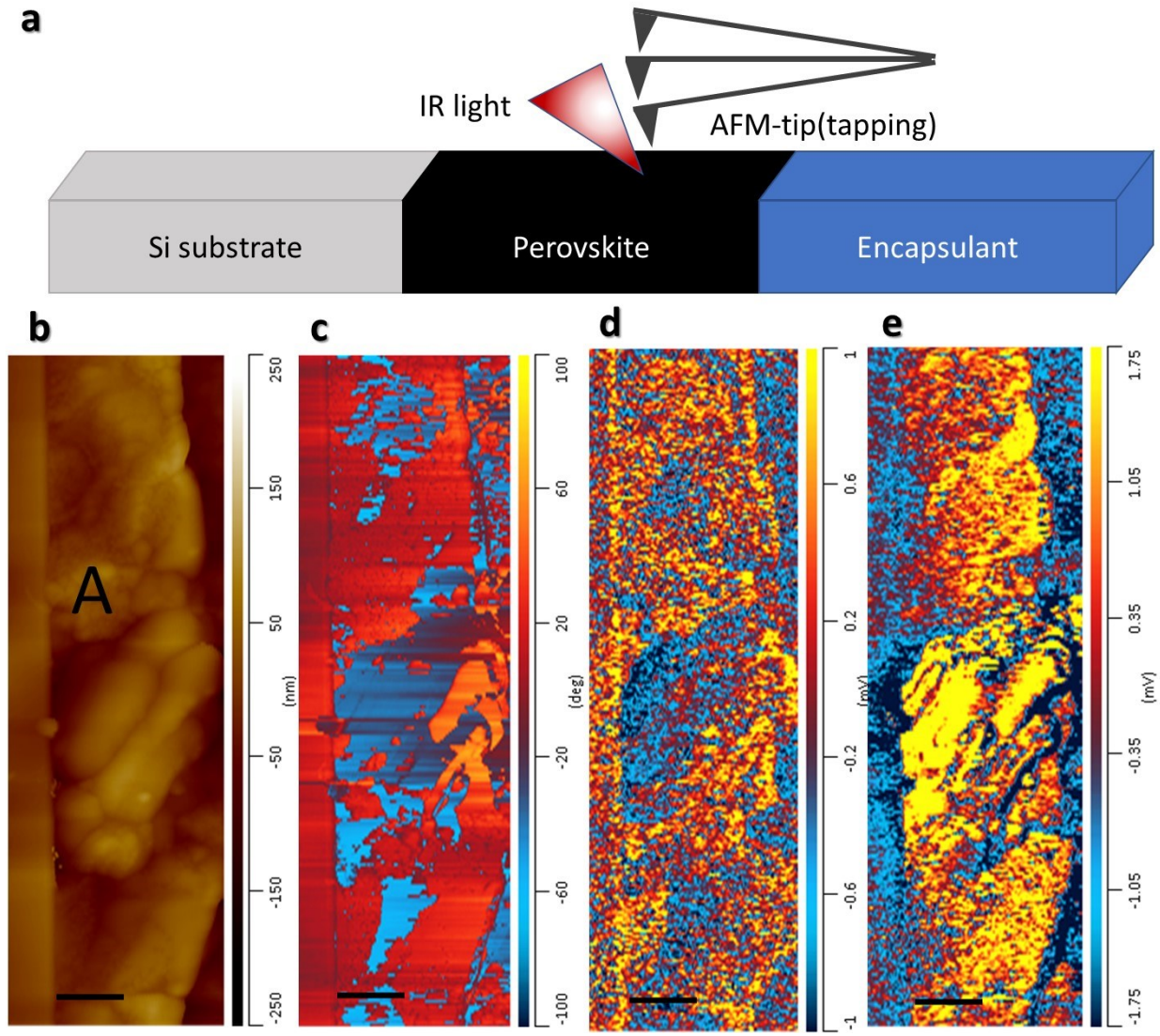

Figure 3. AFM-IR study about cross-section of perovskite films with TPI additive. a) Illustration for the AFM-IR measurement on cross-section area of a sample; b) Topography image of FACs perovskite film with 3% TPI additive; c) Phase image of FACs perovskite film with 3% TPI additive; AFM-IR absorption of FACs perovskite film with 3% TPI additive d) at 975 cm^{-1}, corresponding to $TPPbI_3$; e) at 1713 cm^{-1}, corresponding to FACs perovskite. The length of the scale bar in all figures is 500 nm.

Characterization of perovskite films and devices

We characterized the optoelectronic property of the FACs-perovskite films with and without TPI additives to evaluate the impact of the grain wrapping on FACs-perovskite. The conversion of defective perovskite surface or grain boundaries should also reduce the defects in the perovskite films, which was verified by Photoluminescence (PL) mapping. PL mapping was also used to investigate the non-radiative carrier recombination of perovskite films before and after thermal degradation. **Fig. 4a,b** show that the film with wrapped grains has higher and more uniform PL intensity than the FACs control film. **Fig. S7** shows the PL intensity distribution histogram image of the samples above. The mean value of the emission intensities of the perovskite films with wrapped grains was 2.3 times stronger than the control perovskite film. We estimate that nearly 80% of the perovskite grains have enhanced PL intensity, indicating a grain-wrapping efficiency, and the other 20% are already passivated without grain wrapping. Additional characterizations were performed using the thermal admittance spectroscopy and transient photovoltage (TPV) decay to quantify the effects of grain wrapping on the defect generation and charge recombination dynamics in the devices under operation conditions. Admittance spectroscopy is a well-established method to quantify the trap density of states (t-DOS) in thin-film photovoltaics. As shown in **Fig. 4c**, adding TPI to the FACs perovskites dramatically reduced the trap state density, particularly in the trap depth region of 0.3 - 0.5 eV, which corresponded to the defects of positively charged iodide interstitials(*32*). The TPV decay measurement (Fig. 4d) showed that the carrier recombination lifetime increased from 0.75 μs in the control device to 1.16 μs in the targeted device. Then we encapsulated both films and kept them at 70 ℃ for 456 h in the dark to evaluate the thermal stability. As shown in **Fig. 4e,f**, the emission intensity of the perovskite film with TPI is 1.5 times stronger than the control film after

thermal stress testing, and its average carrier recombination lifetime was also 1.6 times longer than that of the control film. The stronger PL intensity and longer lifetime prove that the grain wrapping slowed down the defects generated during the thermal stress testing.

The TPI in the perovskite films could further reduce the detrimental iodine formation in perovskite during the light-soaking. We immersed FACs perovskite control films and films with different concentrations of TPI (0.6%, 3%, and 6%) into vials filled with 5 ml of TL. Then we illuminated them for seven days under one-sun LED with UV under 55 ℃ in an N_2 filled glovebox. Then we used UV-Visible (vis) absorption spectra to detect the I_2 extracted by the toluene. As shown in **Fig. 4g**, the peak position around 500 nm is used to indicate the I_2 concentration. With the concentration of TPI increasing, the formation of I_2 decreased.

We also measured the whether TPI additives impact strain in the FACs-perovskite films . We compared the XRD pattern of control FACs-peovskite, and those with 0.6% or 3% TPI additive. **Fig. S8** shows that the peak position changes are less than 0.01° after adding TPI, which indicates no extra strain was introduced with the addition of the TPI additive.

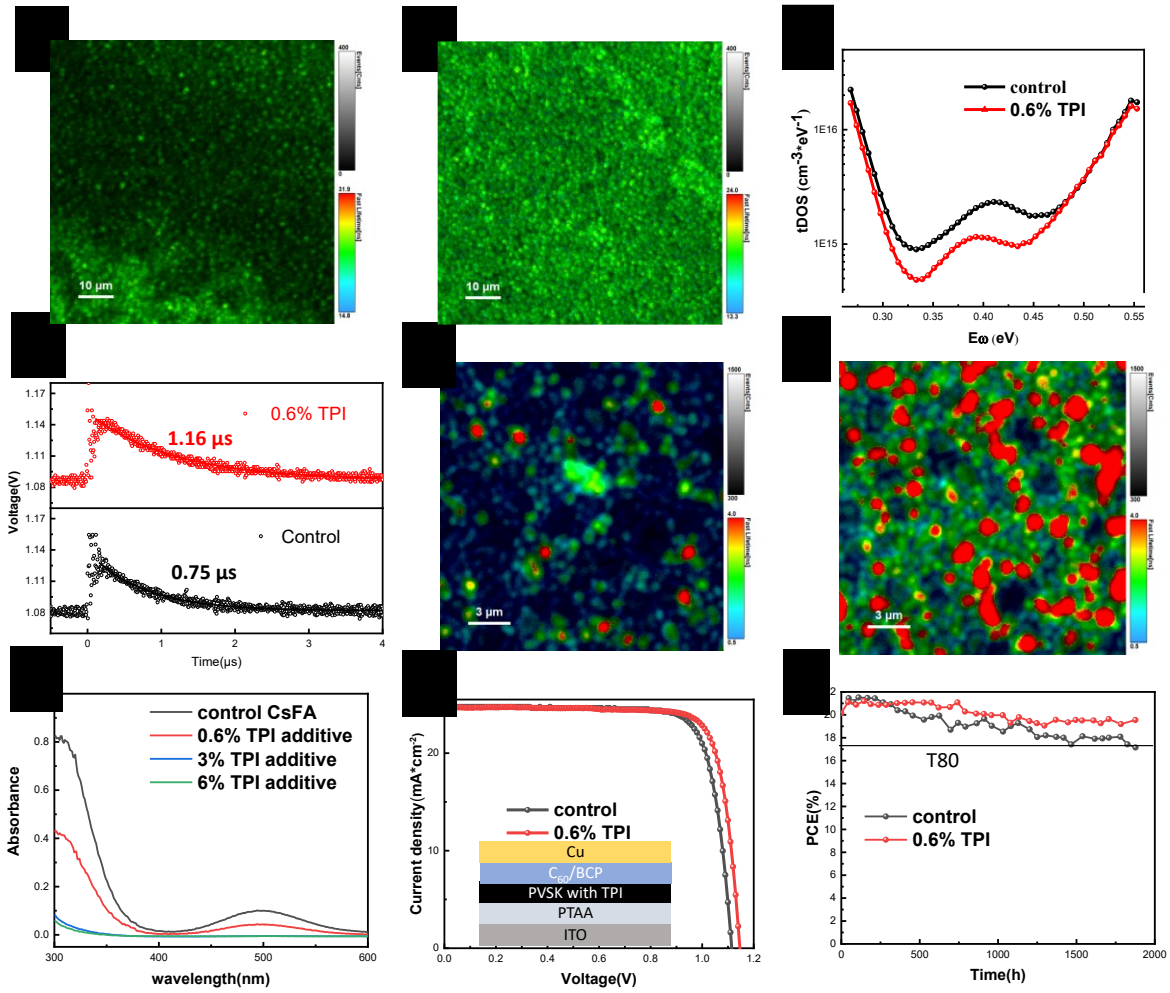

Figure 4. **Performance of Perovskite Devices with Wrapped Grains**. PL mapping of fresh a) FACs control and b)FACs film with 0.6% TPI additive; c) The t-DOS obtained from thermal admittance spectroscopy measurement of the perovskite devices with and without TPI additive; d) Transient photovoltage measurement of devices with and without TPI additive; f) TRPL mapping results of FACs film with the TPI additive under 70 ℃ in the dark for 456 h; e) TRPL mapping results of FACs control film under 70 ℃ in the dark for 456 h; g) UV-Vis absorption of I_2 of films with different concentrations of TPI additives under light soaking degradation; h) J-V curves obtained under AM 1.5 G one-sun illumination at room temperature from FACs control

solar cell and FACs solar cell with 0.6% TPI additive; i) Stability test results of encapsulated control and devices with 0.6% TPI additive under one-sun illumination, 55 ℃, open circuit condition in ambient air.

The photovoltaic performances of devices with and without TPI were then investigated. We applied the grain wrapping technique into p-i-n structure solar cells, employing poly[bis(4-phenyl)(2,4,6-trimethylphenyl)amine] (PTAA) and C_{60} as the hole and electron extraction layers, respectively. A layer of bathocuproine (BCP) was inserted between the C_{60} and copper (Cu) as a buffer layer. The device structure is shown in the inset of **Fig. 4h**. The champion control solar cell without TPI showed an open-circuit voltage (V_{OC}) of 1.11 V, ax short-circuit current density (J_{SC}) of 24.7 mA·cm^{-2}, a fill factor (FF) of 80%, and thus a PCE of 22.0% under air mass (AM) 1.5 global (G) illumination. We optimized the percentage of TPI in perovskite precursors. As shown by the photocurrent curves in **Fig. S9**, too much TPI (e.g. 1.8% mole ratio to lead) would make the device less efficient, mainly due to the insulating nature of TPPbI$_3$, while too less TPI does not really make a difference in device efficiency or stability. The optimal TPI concentration was 0.6 mol% (compared to Pb). After adding 0.6 mol% TPI in FACs-perovskites, the resultant champion PCE was slightly improved to 22.9%, along with an enhanced V_{OC} of 1.15 V, a same J_{SC} of 24.70 mA·cm^{-2}, and a slightly increased FF of 81%. Statistical photocurrent data with twenty devices of each condition is shown in **Fig. S10**; the average PCE was increased from 21.15% to 21.96% by grain wrapping. We also compared the light stability of encapsulated FACs PSCs with and without TPI by light soaking the devices under one-sun illumination for 1900 hours at 55 ℃ in ambient conditions. As shown in **Fig. 3i**, the efficiency of the best control device decreased by 20.3% from its highest PCE after light soaking for 1877 hours. In contrast, the best device with grain wrapping showed only a 7.8% reduction of its highest PCE after light

soaking for the same period. We extracted a duration of 3783 h for the devices that reaches 80% of the highest PCE (T_{80}) for the device with grain wrapping, which is twice longer than the T_{80} of the best control device. It is noted that this stability test was conducted at open circuit condition, which is a more harsh condition than maximum power point tracking.(*45*)

DISCUSSION

In summary, we have demonstrated that adding the tributyl(methyl)phosphonium iodide into FACs perovskite precursor solution to convert the grain boundaries into 1D perovskites can effectively passivate the perovskite grains. This protective layer is robust toward stressors such as heat, light, and moisture, and it can significantly increase the film's thermal and light stability. Moreover, the grain wrapping could dramatically reduce iodide-related defect generation, evidenced by a slowed-down formation of I_2 vapor of the perovskite films under light. After forming the protective layer at grain boundaries, the device could reach 22.9% PCE and a T80 lifetime of 3783 h under light soaking conditions. Adding TPI into the perovskite precursor solution to wrap perovskite grains is a facile way to improve the intrinsic stability of perovskites.

MATERIALS AND METHODS

Materials: Unless stated otherwise, all the materials and solvents were purchased from Sigma-Aldrich. FAI was purchased from GreatCell Solar. CYTOP was purchased from AGC Chemicals Americas, Inc. Epoxy was purchased from Devcon Industries Inc.

Device Fabrication: Indium tin oxide/glass substrates were cleaned with acetone in an ultrasonic cleaner and dried in an oven at 60 ℃; Then, the ITO/glass substrates were treated with ultraviolet-ozone for 15 mins. 2.2 mg/ml PTAA in toluene solution was first blade-coated

without post-treatment for the PTAA film. The perovskite layer was then blade-coated with an N_2 knife blowing at room temperature using a pre-mixed A-B ink.(*39*) A-ink was prepared by dissolving 2.2 M FAI and PbI_2 in 2-ME at room temperature and then further diluted by 2-ME to obtain a concentration of 1.1M according to our previous solvent system recipe. The B-ink was prepared by dissolving CsI and PbI_2 into DMSO at a ratio of 1:1 and stirring the solution at 60 ℃ to fully dissolve the materials at 2.0 M. Formamidinium chloride, phenylethylammonium chloride, and formamidinium hypophosphite added to the A ink as additives at molar percentages of (1.5%, 0.15%, and 1.0%) relative to Pb^{2+} ions, respectively. (Formamidinium chloride and formamidinium hypophosphite were used to passivate non-radiative recombination defects and stabilize the perovskite phase.) TPI, at a molar percentage of 0.6% relative to Pb^{2+} was then added to the mixed solution. The coated around 800 nm thick film was annealed at 150 ℃ for 3 minutes and 100 ℃ for 3 minutes in ambient air to get the perovskite phase. The perovskite film was then thermally evaporated with C_{60} (30 nm), BCP (6 nm), and Cu (150 nm). Finally, the devices were encapsulated by a cover glass with epoxy. The epoxy was then aged for 12 h before characterization.

A thin layer of CYTOP was blade-coated on top of the perovskite film for thermal stability tests.

Fabrication of FTIR sample: 1 mole and 0.5 moles $MAPbI_3$ and TPI were dissolved in 1 ml DMF separately. Pure DMF was used as background, and then we measured the FTIR signal of the 0.5 M $MAPbI_3$ and TPI solutions. Afterward, we mixed the 1 M $MAPbI_3$ and TPI solution at a volume ratio of 1:1 and measured its FTIR.

Single crystal synthesis: We dissolved TPI and PbI_2 in 8 ml 47% HI solution in water with a concentration of 0.5 M. Then, we heated it up to 110 ℃ with stirring. Afterward, we cooled the solution down to room temperature and waited for precipitation.

Fabrication of $TPPbI_3$ film: 0.5 mole PbI_2 and TPI were dissolved in 1 ml DMF. Then we drop 30 μl solution on ITO/glass substrate and spin coat it at the condition of 5000 rpm for 30s. Then we anneal the sample at 100 ℃ for 5 mins.

Characterizations

The J-V curves of perovskite devices were obtained with a Keithley-2400 Source-meter under simulated AM 1.5G irradiation produced by a xenon-lamp-based solar simulator(Oriel Sol3A, Class AAA Solar Simulator). The light intensity was calibrated by a silicon reference cell (Newport 91150V-KG5). The scan rate was about 0.15 $V \cdot s^{-1}$, and only the reverse scan was performed. The device temperature was not controlled during measurement. To measure the long-term operational stability of perovskite solar cells, the devices were encapsulated, illuminated by a one-sun-equivalent LED, and under V_{OC} conditions. Single-crystal XRD measurement was performed on a Bruker SMART Apex II X-Ray diffractometer with Cu Kα radiation (λ = 1.54178 Å). The diffraction data were handled by the Olex2 software,(*46*) and the crystal structure was solved and refined by the ShelXT(*47*) and ShelXL(*48*) programs, respectively. The thermal ellipsoid model was rendered by VESTA.(*49*) The surface AFM-IR was measured by Bruker nanoIR3 with contact mode. The IR laser range was from 900 cm^{-1} to 1900 cm^{-1}. The IR input power is around 0.5% and 0.82%. The measurement was first calibrated by a Polymethyl methacrylate (PMMA) sample for accurate topography, phase, and IR images. After calibration, the control blade-coated perovskite, and spin-coated $TPPbI_3$ films FTIR in the range between 900 cm^{-1} and 1900 cm^{-1} were measured. After selecting distinguished IR peaks: 1713 cm^{-1} for perovskite and 975 cm^{-1} for $TPPbI_3$, topography, phase, and IR image of control perovskite film and perovskite film with 0.6% TPI additive were measured. The cross-section

AFM-IR was measured by Bruker nanoIR3 with tapping mode. The IR laser range was from 900 cm^{-1} to 1900 cm^{-1}. The IR input power range is around 2.1%. The measurement was first calibrated by a PMMA sample for accurate topography, phase, and IR images. After calibration, the perovskite film cross-section sample with a 3% TPI additive was measured. FTIR was measured by PerkinElmer FT-IR spectrometer. The scanning range is from 400 cm^{-1} to 4000 cm^{-1} with a resolution of 4 cm^{-1} and eight scans each time. Film and powder XRD patterns were recorded with a Rigaku Miniflex X-Ray diffractometer. Time-resolved photoluminescence imaging was measured by PicoQuant Micro Time 100 confocal microscopic system. Thermal admittance spectroscopy (*t*-DOS） measurements were performed by using an Agilen E4980A precision LCR meter, and the AC bias amplitude DC bias was fixed at 0 V and the amplitude of the AC bias was 20 mV. The scanning range of the AC frequency was 0.02-2000 kHz. The t-DOS ($N_T(E\omega)$) is calculated by using an equation $N_T(E\omega) = -\frac{1}{qkT}\frac{\omega dC}{d\omega}\frac{V_{bi}}{W}$ where W and V_{bi} are the depletion width and build-in potential, respectively, which were derived from Mott-Schottky analysis of the C-V measurement; q, k, T, ω and C are elementary charge, Boltzmann's constant, temperature, angular frequency, and specific capacitance, respectively. Transient photo-voltage (TPV) decay was measured under 1 sun illumination and recorded by a 1 GHz Agilent digital oscilloscope.

Acknowledgements

Funding: This work is supported by National Science Foundation under award DMR-1903981. The perovskite films preoaring was supported by U.S. Department of Energy's Office of Energy Efficiency and Renewable Energy (EERE) under Solar Energy Technologies Office (SETO)

Agreement Number DE-EE0009520. The views expressed herein do not necessarily represent the views of the U.S. Department of Energy or the United States Government.

Author contributions: H. J. and J. H. conceived the idea and designed the experiments. H. J. fabricated perovskite films and devices. H. J. conducted the XRD, t-DOS, SSPL, PL mapping, FTIR, UV-Vis absorption, AFM-IR and stability measurements. Z. N. and X. D conducted the TPV measurement. Z. S. synthesized perovskite single crystals and carried out single-crystal XRD measurement. H. J., C. F. and Y. L. fabricated the cross-section AFM-IR sample. H. J. and J. H. wrote the paper, and all authors reviewed the paper.

Competing interests: The authors declare that they have no competing interests.

Data and materials availability: All data needed to evaluate the conclusions in the paper are present in the paper and/or the Supplementary Materials.

Correspondence and requests for materials and figures should be addressed to J. H.(jhuang@unc.edu).

REFERENCES

1. H.-S. Kim, A. Hagfeldt, N.-G. Park, Morphological and compositional progress in halide perovskite solar cells. *Chem. Commun.* **55**, 1192–1200 (2019).

2. M. Wang, Z. Ni, X. Xiao, Y. Zhou, J. Huang, Strain engineering in metal halide perovskite materials and devices: Influence on stability and optoelectronic properties. *Chem. Phys. Rev.* **2**, 031302 (2021).

3. A. H. Ibrahim, L. Saad, A. A. Said, M. Soliman, S. Ebrahim, The impact of annealing process on the grain morphology and performance of mesoporous n-i-p carbon-based perovskite solar cells. *AIP Adv.* **12**, 015007 (2022).

4. X. Zheng, B. Chen, J. Dai, Y. Fang, Y. Bai, Y. Lin, H. Wei, X. C. Zeng, J. Huang, Defect passivation in hybrid perovskite solar cells using quaternary ammonium halide anions and cations. *Nat. Energy*. **2**, 1–9 (2017).

5. M. Zhang, M. Ye, W. Wang, C. Ma, S. Wang, Q. Liu, T. Lian, J. Huang, Z. Lin, Synergistic Cascade Carrier Extraction via Dual Interfacial Positioning of Ambipolar Black Phosphorene for High-Efficiency Perovskite Solar Cells. *Adv. Mater.* **32**, 2000999 (2020).

6. Y. Shen, K. Deng, Q. Chen, G. Gao, L. Li, Crowning Lithium Ions in Hole-Transport Layer toward Stable Perovskite Solar Cells. *Adv. Mater.* **34**, 2200978 (2022).

7. Y. Fan, H. Qin, W. Ye, M. Liu, F. Huang, D. Zhong, Improving the stability of methylammonium lead iodide perovskite solar cells by cesium doping. *Thin Solid Films*. **667**, 40–47 (2018).

8. M. Saliba, T. Matsui, J.-Y. Seo, K. Domanski, J.-P. Correa-Baena, M. K. Nazeeruddin, S. M. Zakeeruddin, W. Tress, A. Abate, A. Hagfeldt, M. Grätzel, Cesium-containing triple cation perovskite solar cells: improved stability, reproducibility and high efficiency. *Energy Environ. Sci.* **9**, 1989–1997 (2016).

9. R. Cheng, C.-C. Chung, H. Zhang, F. Liu, W.-T. Wang, Z. Zhou, S. Wang, A. B. Djurišić, S.-P. Feng, Tailoring Triple-Anion Perovskite Material for Indoor Light Harvesting with Restrained Halide Segregation and Record High Efficiency Beyond 36%. *Adv. Energy Mater.* **9**, 1901980 (2019).

10. W. Zhou, Y. Chen, H. Zhou, Strategies to Improve the Stability of Perovskite-based Tandem Solar Cells. *Acta Phys. Chim. Sin.*, 2009044 (2020).

11. N. Ahn, D.-Y. Son, I.-H. Jang, S. M. Kang, M. Choi, N.-G. Park, Highly Reproducible Perovskite Solar Cells with Average Efficiency of 18.3% and Best Efficiency of 19.7% Fabricated via Lewis Base Adduct of Lead(II) Iodide. *J. Am. Chem. Soc.* **137**, 8696–8699 (2015).

12. J. Liu, B. Chen, Q. Wang, R. Li, B. Shi, Y. Li, F. Hou, X. Cui, P. Wang, Y. Li, Y. Zhao, X. Zhang, Self-formed PbI2-DMSO adduct for highly efficient and stable perovskite solar cells. *Appl. Phys. Lett.* **115**, 233901 (2019).

13. S. Chen, X. Dai, S. Xu, H. Jiao, L. Zhao, J. Huang, Stabilizing perovskite-substrate interfaces for high-performance perovskite modules. *Science*. **373**, 902–907 (2021).

14. L. Li, S. Tu, G. You, J. Cao, D. Wu, L. Yao, Z. Zhou, W. Shi, W. Wang, H. Zhen, Q. Ling, Enhancing performance and stability of perovskite solar cells through defect passivation with a polyamide derivative obtained from benzoxazine-isocyanide chemistry. *Chem. Eng. J.* **431**, 133951 (2022).

15. M. Wang, H. Sun, L. Meng, M. Wang, L. Li, A Universal Strategy of Intermolecular Exchange to Stabilize α-FAPbI3 and Manage Crystal Orientation for High-Performance Humid-Air-Processed Perovskite Solar Cells. *Adv. Mater.* **34**, 2200041 (2022).

16. X. Fu, K. Zhou, X. zhou, H. Ji, Y. Min, Y. Qian, Surface passivation for enhancing photovoltaic performance of carbon-based CsPbI3 perovskite solar cells. *J. Solid State Chem.* **308**, 122891 (2022).

17. Y. Zhao, K. Zhao, L. Wan, Y. Tan, Z.-S. Wang, Black Phase of Inorganic Perovskite Stabilized with Carboxyimidazolium Iodide for Stable and Efficient Inverted Perovskite Solar Cells. *ACS Appl. Mater. Interfaces*. **14**, 6906–6915 (2022).

18. Q. Jiang, Y. Zhao, X. Zhang, X. Yang, Y. Chen, Z. Chu, Q. Ye, X. Li, Z. Yin, J. You, Surface passivation of perovskite film for efficient solar cells. *Nat. Photonics*. **13**, 460–466 (2019).

19. T. Niu, Y.-M. Xie, Q. Xue, S. Xun, Q. Yao, F. Zhen, W. Yan, H. Li, J.-L. Brédas, H.-L. Yip, Y. Cao, Spacer Engineering of Diammonium-Based 2D Perovskites toward Efficient and Stable 2D/3D Heterostructure Perovskite Solar Cells. *Adv. Energy Mater.* **12**, 2102973 (2022).

20. A. H. Proppe, A. Johnston, S. Teale, A. Mahata, R. Quintero-Bermudez, E. H. Jung, L. Grater, T. Cui, T. Filleter, C.-Y. Kim, S. O. Kelley, F. De Angelis, E. H. Sargent, Multication perovskite 2D/3D interfaces form via progressive dimensional reduction. *Nat. Commun.* **12**, 3472 (2021).

21. G. Yang, Z. Ren, K. Liu, M. Qin, W. Deng, H. Zhang, H. Wang, J. Liang, F. Ye, Q. Liang, H. Yin, Y. Chen, Y. Zhuang, S. Li, B. Gao, J. Wang, T. Shi, X. Wang, X. Lu, H. Wu, J. Hou, D. Lei, S. K. So, Y. Yang, G. Fang, G. Li, Stable and low-photovoltage-loss perovskite solar cells by multifunctional passivation. *Nat. Photonics*. **15**, 681–689 (2021).

22. S. Yang, S. Chen, E. Mosconi, Y. Fang, X. Xiao, C. Wang, Y. Zhou, Z. Yu, J. Zhao, Y. Gao, F. De Angelis, J. Huang, Stabilizing halide perovskite surfaces for solar cell operation with wide-bandgap lead oxysalts. *Science*. **365**, 473–478 (2019).

23. X. Li, W. Zhang, X. Guo, C. Lu, J. Wei, J. Fang, Constructing heterojunctions by surface sulfidation for efficient inverted perovskite solar cells. *Science*. **375**, 434–437 (2022).

24. J. M. Frost, K. T. Butler, F. Brivio, C. H. Hendon, M. van Schilfgaarde, A. Walsh, Atomistic Origins of High-Performance in Hybrid Halide Perovskite Solar Cells. *Nano Lett.* **14**, 2584–2590 (2014).

25. S. Kundu, T. L. Kelly, In situ studies of the degradation mechanisms of perovskite solar cells. *EcoMat*. **2**, e12025 (2020).

26. N. Aristidou, I. Sanchez-Molina, T. Chotchuangchutchaval, M. Brown, L. Martinez, T. Rath, S. A. Haque, The Role of Oxygen in the Degradation of Methylammonium Lead Trihalide Perovskite Photoactive Layers. *Angew. Chem. Int. Ed.* **54**, 8208–8212 (2015).

27. Q. Sun, P. Fassl, D. Becker-Koch, A. Bausch, B. Rivkin, S. Bai, P. E. Hopkinson, H. J. Snaith, Y. Vaynzof, Role of Microstructure in Oxygen Induced Photodegradation of Methylammonium Lead Triiodide Perovskite Films. *Adv. Energy Mater.* **7**, 1700977 (2017).

28. Y. Zhou, Y. Yin, X. Zuo, L. Wang, T.-D. Li, Y. Zhou, N. P. Padture, Z. Yang, Y. Guo, Y. Xue, K. Kisslinger, M. Cotlet, C.-Y. Nam, M. H. Rafailovich, Enhancing Chemical Stability and Suppressing Ion Migration in CH3NH3PbI3 Perovskite Solar Cells via Direct

Backbone Attachment of Polyesters on Grain Boundaries. *Chem. Mater.* **32**, 5104–5117 (2020).

29. Y. Shao, Y. Fang, T. Li, Q. Wang, Q. Dong, Y. Deng, Y. Yuan, H. Wei, M. Wang, A. Gruverman, J. Shield, J. Huang, Grain boundary dominated ion migration in polycrystalline organic–inorganic halide perovskite films. *Energy Environ. Sci.* **9**, 1752–1759 (2016).

30. J. S. Yun, J. Seidel, J. Kim, A. M. Soufiani, S. Huang, J. Lau, N. J. Jeon, S. I. Seok, M. A. Green, A. Ho-Baillie, Critical Role of Grain Boundaries for Ion Migration in Formamidinium and Methylammonium Lead Halide Perovskite Solar Cells. *Adv. Energy Mater.* **6**, 1600330 (2016).

31. B. Conings, J. Drijkoningen, N. Gauquelin, A. Babayigit, J. D'Haen, L. D'Olieslaeger, A. Ethirajan, J. Verbeeck, J. Manca, E. Mosconi, F. D. Angelis, H.-G. Boyen, Intrinsic Thermal Instability of Methylammonium Lead Trihalide Perovskite. *Adv. Energy Mater.* **5**, 1500477 (2015).

32. Z. Ni, H. Jiao, C. Fei, H. Gu, S. Xu, Z. Yu, G. Yang, Y. Deng, Q. Jiang, Y. Liu, Y. Yan, J. Huang, Evolution of defects during the degradation of metal halide perovskite solar cells under reverse bias and illumination. *Nat. Energy*. **7**, 65–73 (2022).

33. N. Yang, C. Zhu, Y. Chen, H. Zai, C. Wang, X. Wang, H. Wang, S. Ma, Z. Gao, X. Wang, J. Hong, Y. Bai, H. Zhou, B.-B. Cui, Q. Chen, An in situ cross-linked 1D/3D perovskite heterostructure improves the stability of hybrid perovskite solar cells for over 3000 h operation. *Energy Environ. Sci.* **13**, 4344–4352 (2020).

34. E. Ochoa-Martinez, M. Ochoa, R. D. Ortuso, P. Ferdowsi, R. Carron, A. N. Tiwari, U. Steiner, M. Saliba, Physical Passivation of Grain Boundaries and Defects in Perovskite Solar Cells by an Isolating Thin Polymer. *ACS Energy Lett.* **6**, 2626–2634 (2021).

35. T. Kong, H. Xie, Y. Zhang, J. Song, Y. Li, E. L. Lim, A. Hagfeldt, D. Bi, Perovskitoid-Templated Formation of a 1D@3D Perovskite Structure toward Highly Efficient and Stable Perovskite Solar Cells. *Adv. Energy Mater.* **11**, 2101018 (2021).

36. D. Bi, P. Gao, R. Scopelliti, E. Oveisi, J. Luo, M. Grätzel, A. Hagfeldt, M. K. Nazeeruddin, High-Performance Perovskite Solar Cells with Enhanced Environmental Stability Based on Amphiphile-Modified CH3NH3PbI3. *Adv. Mater.* **28**, 2910–2915 (2016).

37. J. Fan, Y. Ma, C. Zhang, C. Liu, W. Li, R. E. I. Schropp, Y. Mai, Thermodynamically Self-Healing 1D–3D Hybrid Perovskite Solar Cells. *Adv. Energy Mater.* **8**, 1703421 (2018).

38. H. Zhang, Z. Shi, L. Hu, Y.-Y. Tang, Z. Qin, W.-Q. Liao, Z. S. Wang, J. Qin, X. Li, H. Wang, M. Gusain, F. Liu, Y. Pan, M. Xu, J. Wang, R. Liu, C. Zhang, R.-G. Xiong, W. E. I. Sha, Y. Zhan, Highly Efficient 1D/3D Ferroelectric Perovskite Solar Cell. *Adv. Funct. Mater.* **31**, 2100205 (2021).

39. Y. Deng, S. Xu, S. Chen, X. Xiao, J. Zhao, J. Huang, Defect compensation in formamidinium–caesium perovskites for highly efficient solar mini-modules with improved photostability. *Nat. Energy*. **6**, 633–641 (2021).

40. A. Dazzi, C. B. Prater, AFM-IR: Technology and Applications in Nanoscale Infrared Spectroscopy and Chemical Imaging. *Chem. Rev.* **117**, 5146–5173 (2017).

41. L. Dimesso, A. Quintilla, Y.-M. Kim, U. Lemmer, W. Jaegermann, Investigation of formamidinium and guanidinium lead tri-iodide powders as precursors for solar cells. *Mater. Sci. Eng. B*. **204**, 27–33 (2016).

42. Infrared and Raman Characteristic Group Frequencies: Tables and Charts, 3rd Edition | Wiley. *Wiley.com*, (available at https://www.wiley.com/en-us/Infrared+and+Raman+Characteristic+Group+Frequencies%3A+Tables+and+Charts%2C+3rd+Edition-p-9780470093078).

43. methyltributylphosphonium iodide - FTIR - Spectrum - SpectraBase, (available at https://spectrabase.com/spectrum/94jZ4exKulc).

44. C. Ge, J.-F. Lu, M. Singh, A. Ng, W. Yu, H. Lin, S. Satapathi, H. Hu, Mixed Dimensional Perovskites Heterostructure for Highly Efficient and Stable Perovskite Solar Cells. *Sol. RRL*. **6**, 2100879 (2022).

45. B. Chen, J. Song, X. Dai, Y. Liu, P. N. Rudd, X. Hong, J. Huang, Synergistic Effect of Elevated Device Temperature and Excess Charge Carriers on the Rapid Light-Induced Degradation of Perovskite Solar Cells. *Adv. Mater.* **31**, 1902413 (2019).

46. O. V. Dolomanov, L. J. Bourhis, R. J. Gildea, J. a. K. Howard, H. Puschmann, OLEX2: a complete structure solution, refinement and analysis program. *J. Appl. Crystallogr.* **42**, 339–341 (2009).

47. G. M. Sheldrick, SHELXT – Integrated space-group and crystal-structure determination. *Acta Crystallogr. Sect. Found. Adv.* **71**, 3–8 (2015).

48. G. M. Sheldrick, Crystal structure refinement with SHELXL. *Acta Crystallogr. Sect. C Struct. Chem.* **71**, 3–8 (2015).

49. K. Momma, F. Izumi, *VESTA* : a three-dimensional visualization system for electronic and structural analysis. *J. Appl. Crystallogr.* **41**, 653–658 (2008).